View metadata, citation and similar papers at core.ac.uk

brought to you by CORE

provided by Open Archive Toulouse Archive Ouverte

Open Archive Toulouse Archive Ouverte

OATAO is an open access repository that collects the work of Toulouse researchers and makes it freely available over the web where possible

This is an author's version published in: http://oatao.univ-toulouse.fr/23399

Official URL:

https://doi.org/10.1016/j.nucengdes.2018.09.003

To cite this version:

Chen, Fang and Allou, Alexandre and Douasbin, Quentin and Selle, Laurent and Parisse, Jean Denis Influence of straight nozzle geometry on the supersonic under-expanded gas jets. (2018) Nuclear Engineering and Design, 339. 92-104. ISSN 0029-5493

Any correspondence concerning this service should be sent to the repository administrator: tech-oatao@listes-diff.inp-toulouse.fr

Influence of straight nozzle geometry on the supersonic under-expanded gas jets

F. Chen[a,b], A. Allou[a,*], Q. Douasbin[c], L. Selle[c], J.D. Parisse[b]

[a] CEA Cadarache, DEN/CAD/DTN/STCP/LTRS, 13108 Saint Paul Lez Durance, France
[b] French Air Force Academy Salon de Provence, Salon Aix 13661, France
[c] Toulouse Fluids Mechanisms Institute UMR 5502, Allée du Pr. Camille Soula, Toulouse 31400, France

ARTICLE INFO

Keywords:
Sodium-gas heat exchanger (SGHE)
Large-eddy simulation (LES)
Under-expanded supersonic gas jets
Taylor-Görtler instability

ABSTRACT

The sodium-cooled fast nuclear reactor (SFR) is one of the most promising designs of the fourth generation (Gen IV) nuclear power reactors. Sodium-gas heat exchangers (SGHE) using nitrogen is being investigated as an alternative to improve operational safety associated with the use of steam Rankine cycles. This alternative eliminates the potential risk of chemical reactions. It is known that cracks inside an SGHE can cause the accidental leakage of nitrogen into the sodium-side. Due to the pressure difference between the secondary and tertiary loops, this nitrogen jet is therefore under-expanded. When the nitrogen leak is strong enough to flush the liquid sodium outside the SGHE channel, the nitrogen jet can be considered as single-phase. In this context, this work focuses on the influence of geometrical parameters of cracks (size, cross-section shape, transverse localization and inclination angle) on the impinging under-expanded nitrogen jet and its shock-wave system. A numerical study of impinging under-expanded nitrogen jet has been carried out using large eddy simulation (LES) technique. We applied a stagnation pressure upstream of the crack of 180 bar while the nozzle pressure ratio (NPR) ranged from 6.0 to 9.2. We were able to identify the link between the nozzle geometry and the Mach disk diameter and its localization. The vorticity distribution at the nozzle can be used to explain the structure of the jets and the entrainment. The central cross-section of the gas jet tends to turn 45° and 90° for square and rectangular cross-section nozzles respectively. The Taylor-Görtler instability is enhanced with a reduction in the nozzle diameter. These instabilities are also increased with square, rectangular and inclined nozzles.

1. Introduction

In sodium cooled fast nuclear reactors (SFRs), equipped with a conventional energy conversion system based on a Rankine cycle with steam, a chemical reaction between sodium and water can occur. In order to avoid this potential event and its deleterious consequences, we decided to investigate innovative energy conversion systems based on a Brayton cycle. This required imagining several types of heat exchangers between the secondary liquid sodium loop and the tertiary inert gas loop. Firstly, within the framework of the Generation IV forum (GIF), the supercritical CO_2 Brayton cycle is currently being investigated due to its very appealing thermodynamic efficiency (*i.e.* up to 44%) com pared with the Rankine cycle (up to 42%). The stability of the whole energy conversion systems based on super critical CO_2 has to be de monstrated. Moreover, if a leak occurs, CO_2 reacts chemically with sodium through an exothermic reaction leading to solid (sodium car bonate) and gaseous reaction products, depending mainly on the local temperature conditions (Vivaldi, 2013; Gicquel, 2010). Nevertheless, the kinetics of interaction are somewhat slower than the sodium water interaction kinetics, thus avoiding any wastage effects (Roger et al., 2014). The sodium gas heat exchanger (SGHE) using nitrogen as inert gas for the secondary loop is also an alternative to a conventional steam Rankine cycle in the short term as it is possible to extract the heat, despite its lower thermodynamic efficiency (up to 38%).

The geometrical description of SGHE is shown in Fig. 1. As we can see in a SGHE module in Fig. 1a, the compact patches form the channels for sodium, which is flowing from left right. While the nitrogen flow crisscrosses the sodium flow, see in Fig. 1b. In addition, the height of the sodium channel is 3 mm where the thickness of the channel is 1 mm. In SGHE channels, the pressures of the tertiary nitrogen loop and the secondary sodium loop are 180 bar and 5 bar respectively, leading to a pressure ratio of 36. The temperatures of two loops are around 753 K and 773 K respectively. A shell crack can accidentally lead to the for mation of an under expanded nitrogen jet into the sodium. In this case,

* Corresponding author.
E-mail address: alexandre.allou@cea.fr (A. Allou).

https://doi.org/10.1016/j.nucengdes.2018.09.003

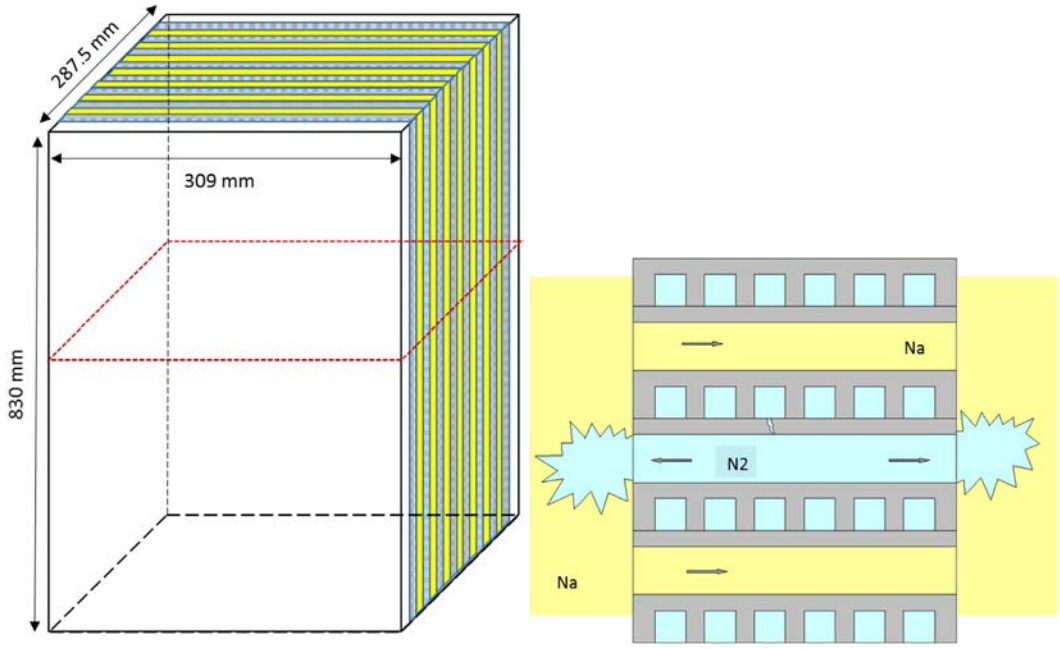

(a) An SGHE module. (b) Cross-section configuration of an SGHE channel.

Fig. 1. Configuration of sodium-gas heat exchangers (SGHE).

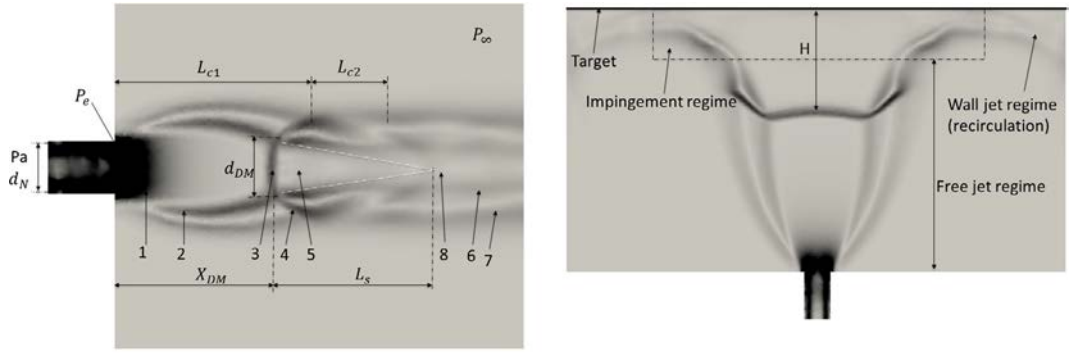

(a) Structure of a free highly under-expanded gas jet. (b) Impinging under-expanded gas jet.

Fig. 2. General structure of under-expanded gas jets. 1: Expanding shock waves; 2: barrel shock; 3: Mach disk; 4: reflected shock; 5: subsonic core; 6: slip line; 7: external boundary of shear layer; 8: supersonic mixing of Mach disk; L_{C1}: length of the first shock cell; L_{C2}: length of the second shock cell; X_{DM}: Mach disk position; d_{DM}: Mach disk diameter; d_N: nozzle diameter; H: distance between the Mach disk localization and the target.

the safety analysis aims at detecting the leak and its impact parameters. Furthermore, according to a numerical study by Vivaldi (2013), it ap proves that the nitrogen leakage can be strong enough to flush the li quid sodium outside of the channel. In the case in point, a steady state under expanded nitrogen jet into a sodium channel can be simulated by a single phase model instead of a two phases model. This means that the sodium side is also initialized with nitrogen. This simplification shortens the computation time. Our work sets out to identify the in fluence of the geometrical parameters of cracks (size, cross section shape, transverse localization and inclination angle) on the impinging under expanded nitrogen jet into nitrogen and its wave system.

An under expanded jet may be formed when a fluid is injected through a crack of a given diameter. We consider a case where the crack exit pressure P_e is greater than the ambient pressure P_∞. The single phase free jet structure mainly depends on the nozzle pressure ratio (NPR) (Love et al., 1959; Cumber et al., 1994; Cumber et al., 1995) and the jet pressure ratio (JPR) (Dam et al., 1998; Crist et al., 1966). The NPR is defined as the ratio between the static pressure at the nozzle exit P_e and the ambient pressure P_∞ (see Eq. (1a)). The JPR is the ratio between the stagnation pressure P_a and the ambient pressure P_∞, (see Eq. (1b)). If the gas flow at the nozzle exit is supersonic, the jet struc ture therefore also depends on the Mach number at the nozzle exit M_e (Antsupov, 1974; Antsupov et al., 1970; Lewis and Carlson, 1964). The nozzle geometry (convergent, divergent or convergent divergent nozzle) and the specific heat ratio also influence the main character istics of the jet (Hatanaka and Saito, 2012; Addy, 1981).

$$NPR = \frac{P_e}{P_\infty}, \tag{1a}$$

$$JPR = \frac{P_a}{P_\infty}, \tag{1b}$$

The structure of free gaseous jets is classified according to the NPR (Cumber et al., 1995):

1. For $1.1 < NPR < 2.0$, the jet is slightly under expanded and has a diamond structure.
2. For $2.1 < NPR < 4.5$, the jet is moderately under expanded and

exhibits a supersonic zone delimited axially by a Mach disk and radially by a barrel shock. This incident shock reflects in a new oblique shock called a reflected shock, facing the outer part of the jet (see Fig. 2a). At the nozzle exit, a Prandtl Meyer expansion fan expands the fluid downstream. The expansion occurs from the lips of the crack up to the external surface of the shear layer. This surface corresponds to the jet boundary. The zone delimited by a white dashed line downstream of the Mach disk is subsonic, while the flow is supersonic upstream of the Mach disk.

3. For 4.5 < NPR < 7, the jet is highly under expanded, and a second shock cell may form. The shape of this shock can be straight or not. The subsonic zone is surrounded by the Mach disk mixing zone delimited by the slip line.
4. For NPR<7, owing to the flowing shock cells downstream of the Mach disk, the Mach disk diameter is smaller or near to the nozzle diameter.
5. For NPR>7, the jet is extremely under expanded and only one normal shock (or one shock cell) is formed, because the first Mach disk diameter is too large to form the second shock cell. Therefore, the Mach disk diameter is higher than the nozzle diameter.

The NPR ranges between 6.0 and 9.2 in this study, thus the jet structures in last two classifications are observed.

Due to the presence of channel walls in the downstream section, the study therefore focuses on an impinging jet. Its structure mainly depends on the NPR, the target inclination and the shape of the target (Kudoh et al., 2013; Donalson and Snedeker, 1971; Donalson et al., 1971; Dauptain et al., 2010; Dauptain et al., 2012). It is characterized by three different regimes (Donalson and Snedeker, 1971): free jet, impingement and wall jet (see Fig. 2b). In the free jet regime, the wall boundary does not affect the jet structure.

Moreover, the vorticity distribution in the shear layer explains the structure of the jet and the entrainment (Totoda and Hiramoto, 2006; Heeb et al., 2014; Liepman and Gharib, 1992). The study of He et al. (2015) describes the characteristics of a supersonic free jet into a liquid through a rectangular nozzle. It is more challenging to observe the Taylor Görtler instability in a shear layer between the nozzle and Mach disk (Arnette et al., 1993; Zapryagaev et al., 2010). In a cross section, the Taylor Görtler vortices are arranged in counter rotating pairs (Görtler, 1954) so that the total pressure distribution looks like a flower petals arrangement (Zapryagaev et al., 2010) (see Fig. 3). Downstream, the development and the merging of these vortices lead to a decrease in their number (Zapryagaev et al., 2010). The Görtler number is the ratio

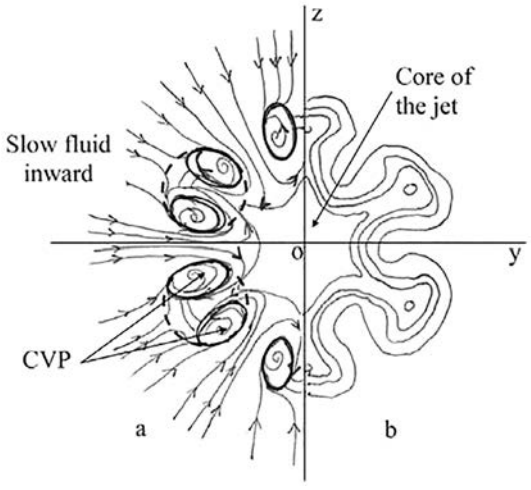

Fig. 3. Schematic of (a) streamlines and (b) distribution of total pressure in the cross section of an under-expanded gaseous jet near the nozzle (Zapryagaev et al., 2010).

between the centrifugal force and the viscous force in the shear layer, defined as:

$$G = \frac{\delta \upsilon}{\nu}\left(\frac{\delta}{\varsigma}\right)^{0.5}. \tag{2}$$

where δ is the momentum thickness, υ the axial velocity, ν the kinetic viscosity and ς the curvature radius. The Taylor Görtler instability can lead to the formation of vortices for $G > 0.3$.

2. Numerical model

The vast literature presenting RANS computations for flows with a high complexity (stemming from either the geometry or the physical phenomena) shows that they are quite sensitive to model parameters. There are usually quite a few constants in RANS models that require tuning to the flow topology (open jet versus internal flows, non reacting versus reacting, etc.). This is the reason for the indisputable success of LES for most practical applications. Recent studies have shown that the LES framework is suitable for the simulation of compressible supersonic impinging jets (Vuorinen et al., 2013; Dauptain et al., 2010; Dauptain et al., 2012). Our work performed with the AVBP code. This code is jointly developed by CERFACS and IFP EN. It solves the compressible Navier Stokes equations on unstructured grids. Integration is performed in the cell vertex formalism with a two step Taylor Galerkin (Colin and Rudgyard, 1993) scheme called TTG4A (Colin and Rudgyard, 2000). This scheme is fourth order in time and third order in space. Closure of the subgrid stress tensor in the momentum equation is performed with the wall adapting linear eddy (WALE) model (Nicoud and Ducros, 1999). An eddy viscosity approach is chosen for the thermal diffusion using a constant Prandtl number, $Pr_t = 0.6$. The TTG4A has very low dissipation and dispersion levels, which is a prerequisite for LES. The downside is its relative lack of robustness in the regions of steep gradients, namely the shocks. Stability is achieved through the addition of bulk viscosity in the regions where numerical errors are detected (Cook and Cabot, 2005).

During operating conditions without defects, the nitrogen side has a pressure of 180 bar and a temperature of 753 K. The sodium side has a pressure of 5 bar and a temperature of 773 K. In order to estimate leakage behaviour, a system mimicking a single SGHE gas channel is modelled by a high pressure reservoir (initial conditions: nitrogen pressure of 180 bar, temperature of 773 K). It feeds one SGHE sodium channel filled by nitrogen through a crack. It is assumed that the equilibrium (pressure, temperature) is achieved between the sodium inside pool (manifold) and the nitrogen inside the leaking channel normally devoted to sodium. The initial conditions for the nitrogen in this channel are: a pressure of 5 bar and a temperature of 753 K.

The dimensions of the channel are: 1 m length (Y direction), 6 mm height (Z direction) and 3 mm width (X direction). The computational domain is shown in Fig. 4. The wall thickness is 1 mm. The general objective of our work is to identify the effect of crack geometry (size, cross section, location and angle) on the development of strongly under expanded gas jets corresponding to a nitrogen leak in an SGHE channel. A crack in this wall is modelled with different cross section shapes: round, rectangular and square. The reference case, denoted D5, consists in a round cross section nozzle with a diameter of 0.5 mm, located at the centre of the channel. The influence of the nozzle size is studied by comparing round cross section nozzles of different diameters (0.28 mm and 1 mm, denoted D28 and D1, respectively) and the reference case D5. Configurations with rectangular (1.5 × 0.3 mm) and square (0.5 × 0.5 mm) cross sections (denoted SR and SC, respectively) were chosen to study the influence of the crack shape. We learned that the Z15 case tends to be off centred by 1.5 mm on the Y axis from the D5 case. And the Y45 case is rotated by 45° around the Y^+ axis from the D5 case. All cases are summarised in Table 1.

Additionally, the present simulations require 3500 14,400 CPU

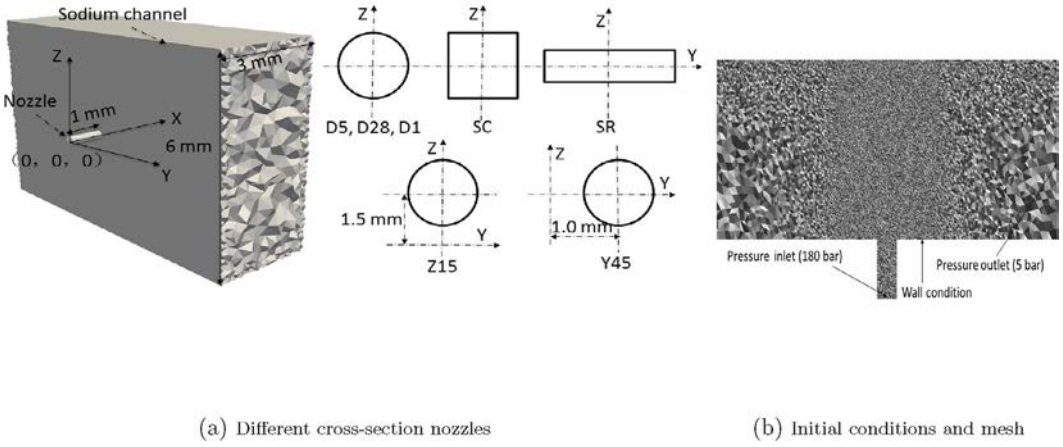

(a) Different cross-section nozzles (b) Initial conditions and mesh

Fig. 4. Schematic of numerical model.

hours for one ms, which means that return times are typically lower than one day for parallel computations on 100 1000 CPUs. For all computations, the mesh resolution is 20 μm in the nozzle and the supersonic jet. This is similar to the work of Dauptain et al. (2010, 2012) who showed good predictions of steady and unsteady features of the jets.

3. Results

3.1. Flow at the nozzle exit

This subsection analyses the differences of the gas flow at the nozzle outlet with respect to its shape. The features of under expanded gas jet are mainly governed by the JPR, the NPR and the Mach number at the nozzle exit as discussed in Section 1. The mean Mach number and central Mach number at the nozzle exit are respectively denoted M_e and M_j. The values obtained from the numerical simulation of these variables are shown in Table 1. M_e and M_j values are greater than 1, which is attributed to a Fanno flow effect. The limited length of the straight orifice involves that the streamlines take a converging/diverging path. It results that the flow accelerates to the supersonic regime.

The theoretical pressure at the nozzle exit can be calculated under the assumption of the incompressible adiabatic flow, see in Eq. (3). For the D5 case, $P_a = 180$ bar and $M_e = 1.152$, the theoretical value is $P_e = 92.6$ bar, thus the NPR is 18.85. For all the cases in the present work, the maximum NPR observed in the simulation is 9.2 (see in Table 1). The maximum value of P_e (NPR × P_∞) is about 52 bar. This lower pressure is due to the compressibility of gas flow. The Y45 case has the weakest NPR; it drops by 27% compared with the D5 case. This suggests that the nozzle length is the most significant parameters for the pressure drop at the nozzle exit. Comparison of the results of the three round cross section nozzles shows that the pressure drop increases with the decrease in the nozzle diameter. The NPR difference between the square (or rectangular) cross section nozzle and the D5 case is about 2.0%. This indicates that the influence of corners in the crack cross section on the pressure drop can be neglected.

$$P_e = P_a \frac{\left(\frac{2}{\gamma+1}\right)^{\left(\frac{\gamma}{\gamma-1}\right)}}{M_e\sqrt{\left(\frac{2}{\gamma+1}\right)\left(1+\frac{\gamma-1}{2}M_e^2\right)}} \tag{3}$$

The Fanno flow effect and the pressure drop influence the structure of the under expanded jet development in the channel. The viscous force inside the nozzle influences the NPR. This latter is linked to the Mach number at the nozzle exit due to Eq. (3). Sections 3.2 and 3.3 show that the NPR and the Mach number M_e control most of the characteristic lengths described in Fig. 2a. It will be then shown in Section 3.5 that the Mach disk shape is a consequence of the vorticity inside the nozzle. This vorticity is created by the actions of viscous forces in the boundary layer. Thus all the geometrical features of the jet are controlled by the drag forces at the wall inside the nozzle.

3.2. Qualitative analysis of jet shapes in longitudinal cuts

Owing to the different NPR for each case described in the previous subsection, under expanded nitrogen jets can be classified into 2 groups. Fig. 5 shows longitudinal cuts of the norm of the density gradients for all cases. As discussed in Section 1, a classification based on the NPR allows us to distinguish the different jet shapes. From Table 1, 6.0 < NPR < 9.2.

1. For cases D28 (see Fig. 5b) and Y45 (see Fig. 5d): 4.5 < NPR < 7.

Table 1
Mean values over cross-section for each simulation result case.

	Size			Localization	Inclination	Shape	
Nomenclature	D5	D28	D1	Z15	Y45	SC	SR
D_N (mm)	0.5	0.28	1.0	0.5	0.5	0.5	0.5
Nozzle Shape	Round	Round	Round	Round	Round	Square	Rectangular
Nozzle exit (y,z)	(0, 0)	(0, 0)	(0, 0)	(0, 1.5)	(1.0, 0)	(0, 0)	(0, 0)
M_e	1.152	1.057	1.238	1.173	1.176	1.160	1.075
M_j[a]	1.39	1.47	1.34	1.39	1.44	1.41	1.33
NPR	8.22	6.89	9.18	8.10	6.0	8.0	8.98
JPR	15.77	12.21	18.84	15.81	9.89	15.4	16.1
H[b]/D_N	6.0	10.7	3.0	6.0	6.5	6.0	6.0

[a] Mach number at central streamline at the nozzle exit.
[b] Distance between nozzle exit and target.

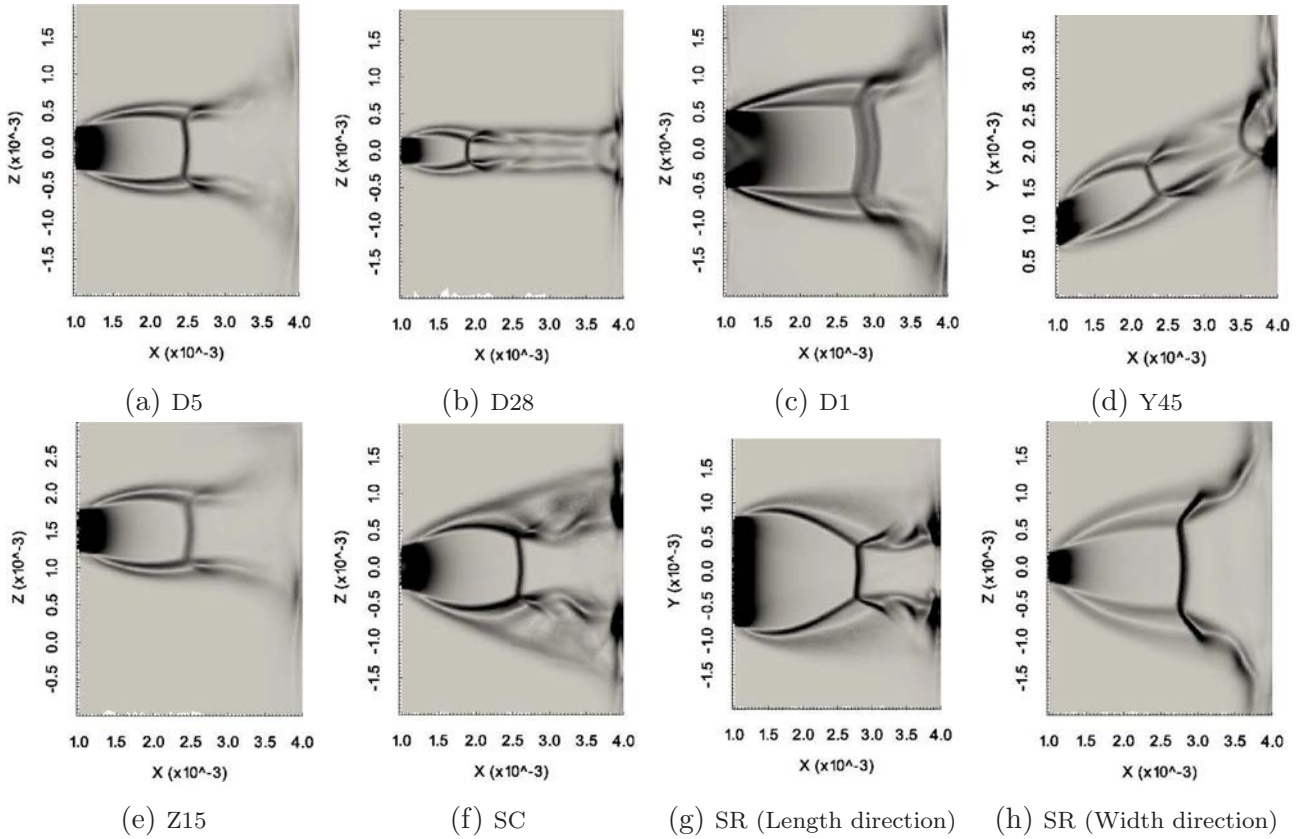

Fig. 5. Longitudinal cuts of the norm of the density-gradients show the expansion of the jets. Minimum and Maximum values of the colour bar is respectively 100 and 8 10^4.

Table 2
The Görtler number at the 0.2 mm to the nozzle exit.

	*D*5	*D*28	*D*1	*Z*15	*Y*45 (Y[+a])	*Y*45 (Y [b])	*SC*(*Z*)	*SC* (*diag*[c])	*SR*(*Y*)	*SR*(*Z*)	*SR* (*diag*[d])	*SC* (*vortex*)[e]
δ (mm)	0.0192	0.0209	0.0164	0.0180	0.0151	0.0151	0.0173	0.0091	0.0189	0.0264	0.0208	0.0255
ς (mm)	0.7545	0.8271	0.8241	0.9606	1.5384	5.1609	1.8987	2.4576	1.1305	1.2746	1.4812	1.2369
U (m/s)	954	977	876	965	986	945	935	926	939	903	915	933
G	673	743	456	547	337	176	356	117	528	787	517	782

[a] Inclined direction.
[b] Opposite inclined direction.
[c] Corner position of square cross-section nozzle.
[d] Corner position of rectangular cross-section nozzle.
[e] One vortice localisation of square cross-section nozzle.

Double shock cells and a subsonic zone behind the Mach disk can be observed. The supersonic mixing zone can be seen downstream of the Mach disk if confinement due to the channel wall is minor. Consequently, the flow is supersonic at the impingement on the target. For case Y45, the nozzle inclination induces asymmetry in the jet, which develops more in the direction of positive Y (see Fig. 5d). Moreover, the stagnation point is not aligned with the channel axis and is located at Y = 2.3 mm instead of Y = 4.0 mm. This observation is consistent with the experimental study of Donalson and Snedeker (1971), which shows that the stagnation point at the target displaces with the inclination angle increase. The curvature in the inclination direction is 0.65 mm^{-1}, which is larger than that in the opposite direction: 0.18 mm^{-1}) (see Table 2). This is an important parameter for the development of the Taylor Görtler instability (see Eq. (2)).

2. For all other cases: 7 < NPR < 10. Only the first shock cell is ob served. All the cases are symmetric on the XZ plane. Supersonic expansion and re compression zones can be observed behind the shock cell. The gas flow is subsonic in the vicinity of the impact on the target. The most intensive pressure gradients on the target are located in a circle. The centre of this circle is located at the inter section of the target and the axis symmetry of the nozzle. The re circulation of a strong jet around the Y axis can be seen in cases D1 and SR. Otherwise, further analysis of case SC illustrates that the shear layer is rectilinear shape and diverges with an angle of 26°, as shown in Fig. 5f. This feature is close to the angle of 24° reported for a gaseous jet in liquid sodium (Roger et al., 2014). In addition, the reflected shock waves in the shear layer downstream of the Mach disk increase the jet diameter. In contrast, the flow is convergent on the diagonal plane because of the corners in the cross section, this phenomenon agrees with the numerical observations of He et al. (2015). The barrel shock is straight for the D1 case, for the other cases the barrel shock is curved. For case SR, the barrel shock is divergent from the nozzle widths; conversely it is convergent on the nozzle lengths and the corners. It shows that the flow develops more strongly in the direction of the nozzle width than length.

In conclusion, the general structures of the gaseous jets are in good agreement with the theoretical classification, which provides a quali tative validation of the numerical model. For a rectangular nozzle, the structure of the barrel shock is convergent and divergent on two sym metric planes.

3.3. Mach disk

Firstly, this part aims to validate the numerical model by comparing the simulation results with the existing theoretical or experimental correlations. Secondly, the influence of the nozzle geometry on the main characteristics of the under expanded jet will be identified by comparing the numerical results with a reference case. The gas leak can be detected by an acoustic method based on the Mach disk structure (Cavaro, 2010). Therefore, the Mach disk characteristics are some of the most useful input data for leak detection. Thus, the Mach disk lo calization and diameter are selected to validate the numerical model and identify the influence of the nozzle geometry on them.

3.3.1. Mach disk localization

Among the parameters commonly used to describe the under ex panded gas jet, Mach disk localization has been largely studied. For the free jets, the experimental work of Love et al. (1959) studies the di mensionless localization of the Mach disk as a function of the NPR. This experiment used air gas injected through convergent and convergent divergent nozzles. In this study, the M_j values range from 1.0 to 3.0. The NPR values range from 1 to 120.

The correlation proposed by Lewis and Carlson (1964) integrates the Mach number at the nozzle exit and the specific heat ratio γ, shown in Eq. (4). This equation is taken from the experiments for a range:

1. γ from 1.22 to 1.67.
2. Mach number from 1 to 3
3. NPR from 1 to 550.

These two experimental studies show that the Mach disk localiza tion increases with the NPR and the Mach number.

$$\frac{X_{DM}}{D_N} = 0.69 M_j \sqrt{NPR\gamma} \tag{4}$$

In Fig. 6a, the dimensionless localizations of the Mach disk obtained from an SGHE channel model are compared with the values obtained from free jets experiments. The numerical value obtained for the D1 case is weaker than both experimental results, with a maximum error of 88%. In Table 1, it can be seen for the D1 case that the dimensionless distance between the localization of the Mach disk and the wall of the channel is the lowest (*i.e.* 3.0). This means that the channel confine ment effect is the strongest. This is why in this case the Mach disk lo calization is lower than the experimental values obtained from the free jets. For the others cases, the numerical results are more consistent with the experimental results of Love et al. (1959) and the correlation of Lewis and Carlson (1964). The maximum error is 11.3% and 5.0%, respectively. The mean error is 7.3% and 3.3% respectively. It proves that the Lewis' correlation is more suitable for reproducing the data of our numerical model. This capability is due to the explicit integration of the Mach number into the correlation. As detailed in Section 3.1, the pressure drop inside the nozzle prevents us from estimating the Mach number at the nozzle exit (M_e) using only P_a and P_∞. Moreover, im posing an exact M_e is the most efficient method for taking into account the pressure drop due to the nozzle. Having an exact Mach number will produce more detailed results for each case. Lewis' correlation through M_e takes into account the viscosity effect inside the nozzle. The nu merical results are very similar to this correlation, considering that the numerical model is accurate enough to be used for studying leaks in SGHE.

The nozzle location has no considerable effect on the Mach disk X_{DM}. In the Y45 case, the nozzle inclination decreases the distance between the nozzle exit and the Mach disk owing to the NPR decline. Another reason is the presence of the second shock cell (Heeb et al., 2014) which also decreases this distance.

The D5, Z15, Y45, SC and SR cases have the same hydraulic dia meter of 0.5 mm (see Table 1). The rectangular cross section nozzle enlarges $\frac{X_{DM}}{D_N}$ by 13% when compared with all the other cases. Ac cording to Fig. 5h, this enlargement is caused by the gas flow devel opment toward the exterior in the width direction. Then the 2D struc ture is divergent in this direction (see Fig. 5h); this divergence will enlarge the X_{DM}. The square cross section nozzle enlarges this distance by 5% when compared with the reference case D5.

3.3.2. Mach disk diameter

In the safety analysis of SFRs, it is shown that the Mach disk dia meter can be correlated with acoustic noise generated by the gas jet (Cavaro, 2010). This means that any accidental effects (*i.e.* mass flow of nitrogen, crack size) can be deduced knowing the diameter of the Mach disk, which is a substantial research subject for an accident in an SGHE. In this subsection, the influence of the nozzle geometry on Mach disk diameter will be shown. In Fig. 6b, the hydraulic diameter of the Mach disk is calculated for the rectangular and square cross section nozzles. The Mach disk diameter increases with the JPR or the NPR. Love et al. (1959) also proposed the variation in the Mach disk diameter as a function of the NPR thanks to the experiment mentioned in the previous section. Another empirical correlation proposed by Antsupov (1974) can be used to fit the data obtained from numerical model in Eq. (5).

$$\frac{D_{DM}}{D_N} = \frac{0.65}{M_j}(NPR - 0.55M_j)^{0.62} \tag{5}$$

The numerical and empirical results are shown in Fig. 6b.

The numerical results of the SC, Z15, D5 and SR cases agree with the correlation of Antsupov (1974) and of Love et al. (1959), as shown in Fig. 6b. The maximum error compared with these experimental

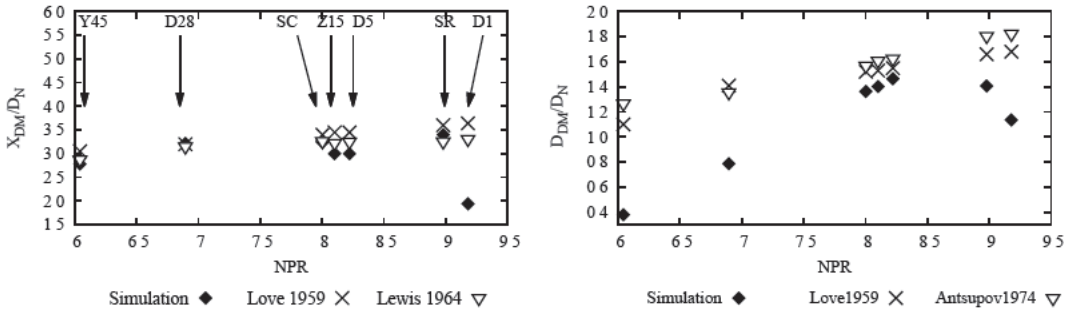

(a) Mach disk dimensionless localization

(b) Dimensionless diameter of the Mach disk

Fig. 6. Comparison between the simulations results and the reference values.

correlations is of 28% and 18% respectively for these four cases. Moreover, the rectangular and square cross section nozzles decrease the diameter of the Mach disk due to the re compression of the shock waves downstream of the Mach disk. The numerical value of the D1 case differs from the experimental correlation of 60%. This is due to the strong reflected shock waves from the target. The D28 case has a dif ference of 80% comparing with the experimental data. Nevertheless, the result in present work is still reliable, because the Mach Disk dia meter is smaller than the nozzle exit one where the NPR of case D28 is in the range between 4.5 and 7, the result of D28 agrees with this classification. In addition, the minimum diameter investigated in these experiments is 0.66 mm. Then the diameter of 0.28 mm falls out of the confidence domain of use of empiric correlation. The value of the Y45 case contrasts the most with the empirical result, with a difference of about 200%. It means that the inclination nozzle therefore has the longest influence on the Mach disk diameter.

In conclusion, the numerical model is validated through:

1. 2D structures of the gas jets,
2. Comparison between the numerical results and the experimental values.

The influence of the nozzle geometry on the dimensionless diameter of the Mach disk is more sensitive to $\frac{D_{DM}}{D_N}$. The rectangular cross section nozzle has a greater effect on the localization of the Mach disk than the square cross section nozzle. Inversely, the square cross section nozzle decreases the Mach disk diameter more significantly than the rectan gular cross section nozzle. This means that the nozzle's aspect ratio has a greater effect on the localization of the Mach disk than the Mach disk diameter. The nozzle inclination has the strongest effect on the jet feature. The channel confinement effect is significant for the D1 case.

3.4. Jet diameter evolution

The jet diameter is a key parameter for determining the jet's area of influence in the sodium channel. This part of the paper discusses the jet diameter with respect to the streamwise direction. Qualitatively, it in creases with the NPR and the Mach number at the nozzle exit (Love et al., 1959; Avduevskii et al., 1970). In the present work, the jet dia meter is estimated by using the radial profile of the dimensionless pressure P/P_t. Where P_t represents the total pressure at the nozzle exit. An example is given in Fig. 7a for the SC case. The global minimum pressure is considered as the boundary of the gas jet, noted point C in Fig. 7b. There is a local minimum value of the dimensionless total pressure for all the studied cases, noted point A. This minimum di mensionless pressure coincides with:

1. The barrel shock localization upstream of Mach disk

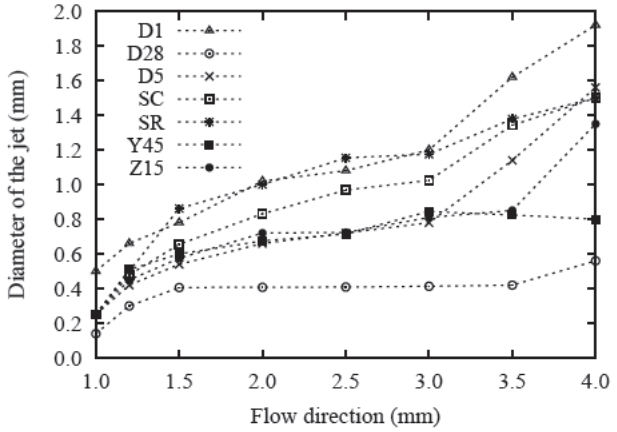

Fig. 8. Evolution of the dimensionless hydraulic diameter of jet in terms of the flow direction.

2. The subsonic region boundary or slip line downstream of Mach disk.

The maximum dimensionless pressure coincides with the internal boundary of the shear layer, noted point B. The point D represents the second local maximum of the total pressure. It is derived from the re compression shock waves.

The jet hydraulic diameter variation is estimated by using the po sition of point C (see Fig. 7b), the profile is shown in Fig. 8. In the region adjacent to the nozzle exit, the SR, SC, Z15 and Y45 cases have a diameter which increases more sharply than the reference case D5. This feature corresponds to the jet structures shown in Fig. 5. At the outlet of the nozzles, the barrel shock structures of case D1 and D28 are straighter than the other cases (data not shown).

In this region of the Y45 case, the slope of the jet diameter change is the sharpest. In this case, the second shock cell reduces the Mach disk localization $\frac{x_{DM}}{D_N}$ and increases the diameter of the jet. Downstream, the diameter does not increase as sharply, especially for the D28 case where it remains close to constant. Downstream, the jet diameter has a ten dency to be constant with the decrease in the nozzle diameter. Generally, the Z15 case possesses the same tendency as the reference case. The rectangular nozzle significantly enlarges the jet diameter compared with the reference case D5, because the NPR of this case increases the most. The barrel shock is divergent in the width direction (Fig. 5h), which implies an increase in the jet diameter. The square nozzle increases the hydraulic diameter compared with the reference case D5, because the reflected shock waves in the shear layer (see Fig. 5f) increase the jet diameter.

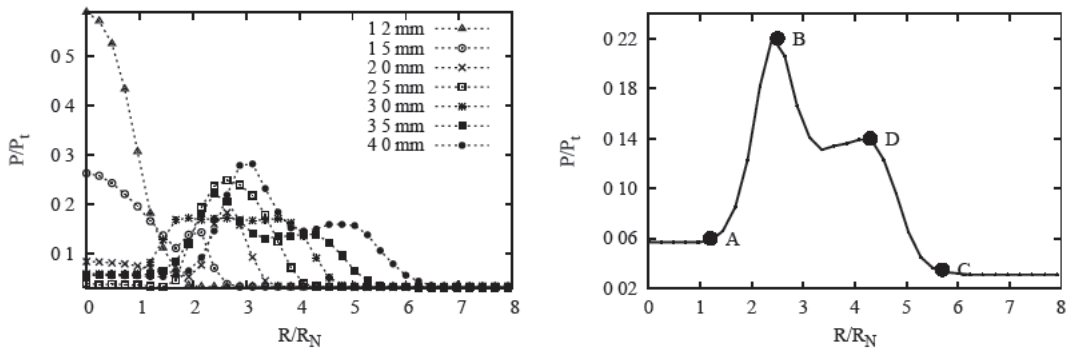

(a) Radial pressure profiles for different axial positions.

(b) An example for x=3.5 mm of SC

Fig. 7. Radial profiles of the dimensionless total pressure for the SC case.

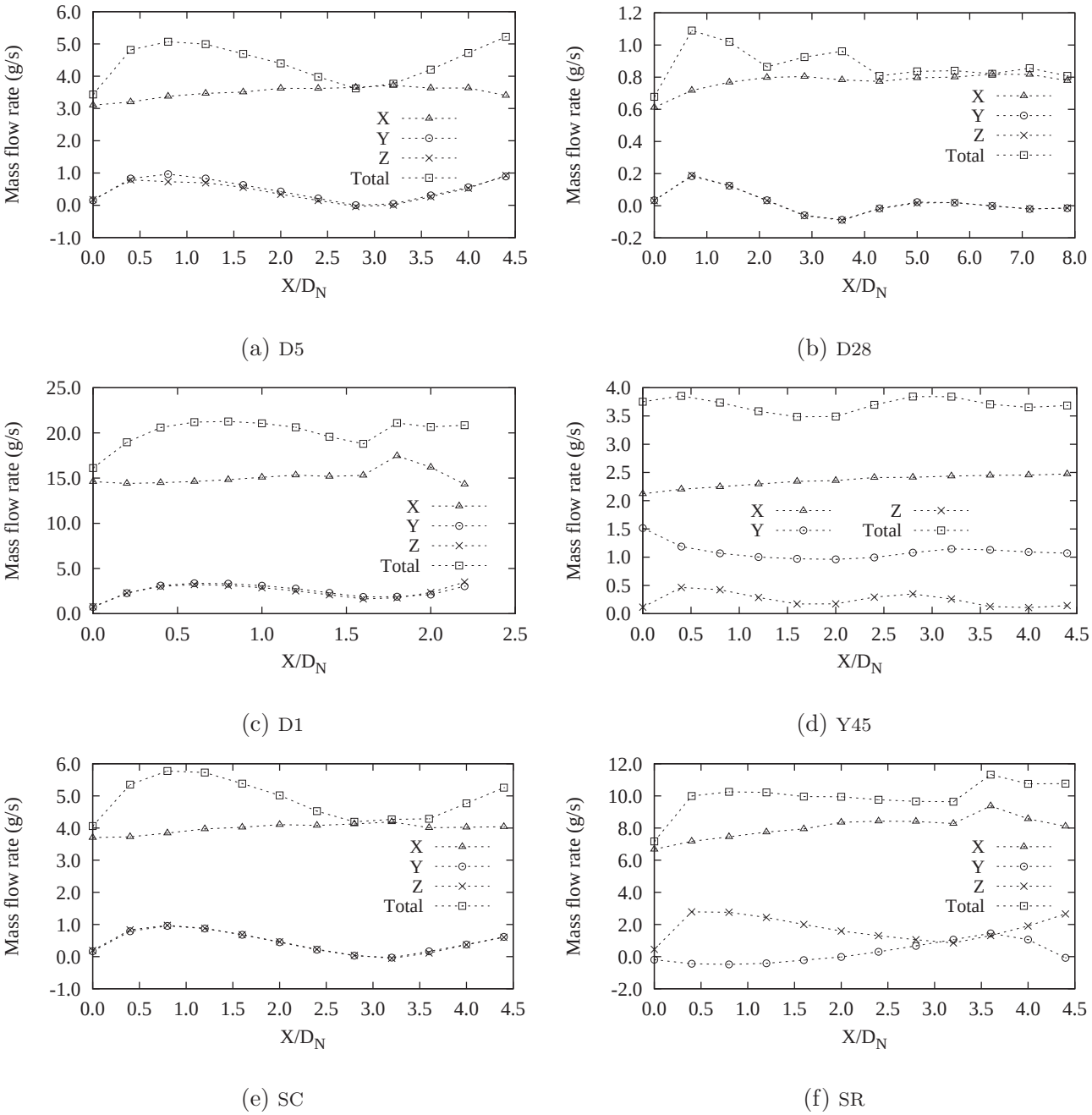

Fig. 9. Variation in the mass flow as a function of the flow direction.

3.5. Mass flow rate and cross section shape

In the safety analysis of the SGHE in SFRs, detecting the mass flow rate of the nitrogen jet is one of the most substantial objectives. Being able to predict the impinging pattern is also an appealing goal in order to evaluate its effect on the sodium channel. Consequently, this section investigates the mass flow rate and the cross section shape of the jet. Fig. 9 shows the mass flow variation along the flow direction. For all the cases, the mass flow in the X direction remains constant in the vicinity of the nozzle exit. At this point, the mass flow rate is 4, 16 and 0.7 g/s for the nozzle diameters of 0.5, 1.0 and 0.28 mm respectively. This means that the mass flow rate is proportional to the cross sectional area of the nozzle. Therefore, the variation in the $\rho\upsilon$ term (ρ and υ represent the density and velocity of the gas flow respectively) is identical for all the cases.

The mass flow rate reaches its maximum at a distance of one nozzle diameter from the nozzle outlet. It is due to ambient gas entrainment. In the downstream of the nozzle, the mass flow rate slowly increases owing to the jet recirculation near the target.

The variation in the jet structures defined by the $\rho\upsilon$ term shown in Fig. 10. Downstream, significant $\rho\upsilon$ values develop towards the outer part of the jet. This implies a change in the mass flow distribution from a central concentration of 80%, towards the periphery of the jet with 60% of the total mass flow. This profile is inverse to the velocity profile which means that the density change is predominant. However, downstream of Mach disk, it becomes concentrated once again in the central jet (seen in the D28 case in Fig. 10b). This pattern agrees with the experimental study of target wastage shape in the case of a nitrogen jet submerged in liquid sodium (Lécume et al., 1989). For the other cases, the profile of $\rho\upsilon$ re concentration is not observed, due to the short distance between the Mach disk and the target (Table 1).

In the region adjacent to the nozzle exit, the cross section shape of

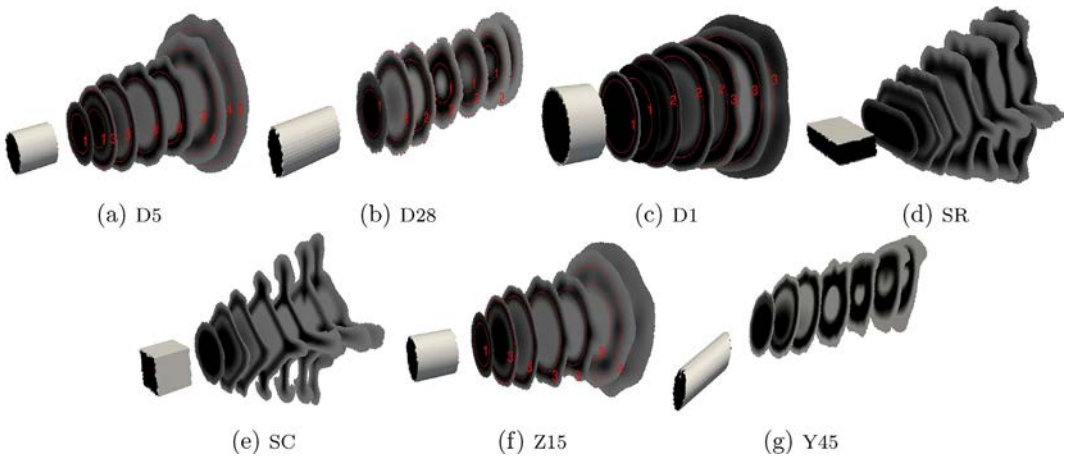

Fig. 10. Variation in jets defined by the $\rho\upsilon$ term. 1: $r/r_N = 1.0$, 2: $r/r_N = 1.5$, 3: $r/r_N = 2.0$, 4: $r/r_N = 2.5$, 5: $r/r_N = 3.0$. Maximum and minimum value of the colour bar is 1.6e3 and 4e3 respectively.

jet is similar to the nozzle cross section through which it is injected. For each case shown in Fig. 10, the fourth cross section slice in the flow direction represents the Mach disk. In the vicinity of the Mach disk, the jet shape is disturbed; these disturbances coalesce downstream of the Mach disk. The jet deformation is the strongest in the SR and SC cases. Downstream of the Mach disk, the jet cross section shape of the D28 and Y45 cases remains the same as that at Mach disk, as seen in Fig. 10b and g. For the Y45 case, however, the gas flow is more disturbed due to the inclination of the nozzle compared with the D28 case. In the SC case, the mass flow develops from the centre to the fours edges of the nozzle respecting the nozzle cross section shape. The central jet shape is round at the nozzle exit (see Fig. 10e) and then square which turns 45° compared with the cross section of the nozzle. Farther downstream, the central cross section of the jet looks like a cross. In the SR case (see Fig. 10d), the mass flow develops from centre to the four edges of the nozzle as in the SC case. For the SR case, the gas flow develops more along the width direction (Z axis) than the length direction (Y axis). The cross section jet shape downstream has a 90 degree rotation compared with that upstream. Along the width direction, three disturbance peaks can be seen; one disturbance peak is observed in the length direction. This pattern is completely different from the observations in the SC case. This illustrates that the disturbances are more intense along the width direction of the nozzle.

Fig. 10 allows us to identify the development of the $\rho\upsilon$ term. Near to the nozzle exit, in a flow cross section, the most part of the $\rho\upsilon$ passes through a small area. This area is defined by the contour of level 1: $r/r_N = 1$, where r_N is the nozzle radius. At a distance of about one nozzle diameter from the nozzle exit, most of the $\rho\upsilon$ term is concentrated around the radial coordinates $r/r_N = 3$. Downstream, this area of strong $\rho\upsilon$ term convergences on the centre line. This streamwise pattern is also observed in the total pressure profile, as seen in Fig. 11. For a given cross section (Mach disk position), the profiles of $\rho\upsilon$ in Fig. 10 and the contour of total pressure in Fig. 11 are identical. Then the dynamic pressure leads the free jet regime by the means of density changes as stressed out above. This fact was also observed (Zapryagaev et al., 2010) experimentally. For all the round cross section nozzles, the cross section shape of the Mach disk is the same as the nozzle cross section shape. However, it is different for the SR and SC cases. Furthermore in these two cases, the Mach disk shape of the SC case shown in Fig. 11d apparently turns 45° compared with the nozzle cross section. In the case of the rectangular nozzle shown in Fig. 11c, the Mach disk apparently turns of 90°.

In addition, the total pressure are perturbed on the jet boundary for the round cross section nozzle. For the Y45 case, the total pressure contour has the same pattern with reference one in the opposite in clination direction (Y^-), see in Fig. 11b. Meanwhile, the maximum total pressure in the inclination direction (Y^+) has three picks. The dis tribution of the total pressure of the SC case has a cross shape, as shown in Fig. 11d. For SC case, the maximum total pressures are located at four cardinal points. Compared with the SC case, the maximum total pressures of the SR case exhibit a different pattern. This is due to the more intensive development of the gas flow in the width direction than in the length direction.

In order to explain the cross section shape of the jet, the vorticity profile over the rectangular and square nozzles is studied in a cross flow section located in the middle of the nozzle length. This location is far from the inlet and the outlet to avoid section change effect. The vor ticity near the edges (0.05 mm from the edges) of this section and the vorticity of the diagonal over this cross section are plotted, as shown in Fig. 12.

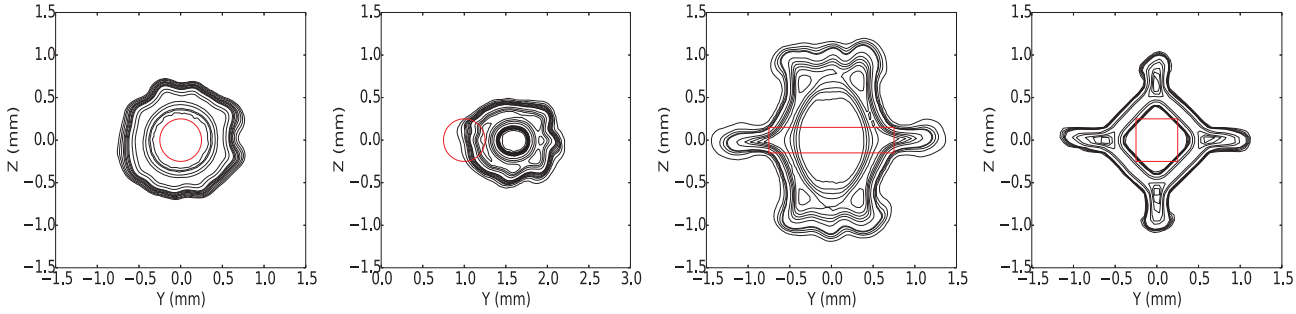

Fig. 11. The total pressure pattern in the Mach disk localisation. The red curves are the initial cross-section of nozzles.

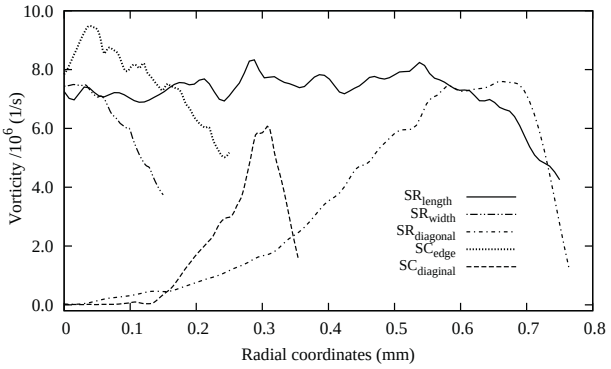

Fig. 12. Vorticity distribution in the square and rectangular nozzles.

In the centre of the gas flow, the vorticity is around zero. This proves the presence of a potential region. On all edges of the nozzle, the gas flow develops outwards after the nozzle exit due to the high vor ticity. The maximum value in the diagonal line is lower than that along the edge. The vorticity in the corners is 5 times lower than that at the edges. Then the gas flow from the nozzle exit develops less in the corners than in the edges. For the square nozzle, the norm of vorticity is higher on each edge than on corners. It exhibits a local maximum near the middle of each edge. This will reshape the cross section of jet comparing with the one of nozzle. Indeed, for each edge, the flow at each maximum of vorticity will be strained the most in the radial di rection. Then each maximum of vorticity represents a new corner. Quadrangle that links the four new corners is necessary square because the maximums of vorticity are the same at the four edges of the nozzle exit. The reshaped cross section turns of 45° comparing to the initial nozzle one, because the angle between the position of maximum of vorticity in the edge (near to the middle) and the nozzle corner is of 45°, see in Fig. 12. Due to the same for the SR case, the norm of vorticity in the length edge is higher than the one in width edge; this is why the cross section of jet in downstream will change of 90° comparing the initial nozzle shape.Fig. 13.

3.6. Taylor Görtler instability

The flow pattern exhibits vortices caused by instabilities in the vi cinity of the jet. Due to the strong curvature provoked by the features detailed in Section 3.2, we chose to focus our research on the Taylor Görtler instabilities. The methods for vortice identification are based mainly on the velocity gradient tensor ($Q_{criterion}$, $\Delta_{criterion}$) (Kolr, 2007), vorticity (Kida and Miura, 1998; Moin and Kim, 1985) or directly from the velocity field (Zhou et al., 1999; Holmen, 2012). A more complex method aims at identifying the central position and the intensity of the vortices (Graftieaux et al., 2001). A Görtler number G (Eq. (2)) higher than 0.3 is a necessary condition for the formation of Taylor Görtler vortices in a counter rotating pair shape. Nevertheless, this condition is insufficient to observe these vortices.

The Taylor Görtler vortices are generated at the nozzle exit, the Görtler number is thus studied at 0.2 mm downstream of the nozzle exit (data in Table 2). We consider that the possibility of vortices formation at a given X position for the round cross section nozzles is uniform at radial circle, the Görtler numbers in Z^+ direction are studied. For the Y45 case, the Görtler at the inclined direction (Y^+) et its opposite di rection (Y^-) is respectively studied. The Görtler numbers in Y, Z and the diagonal directions are calculated for SR and SC cases. In addition, the position of vortices of SC case are not exactly located at the centred edge according the vorticity distribution in Fig. 12, because the max imum norm of the vorticity is lightly centre off. A centre position of the Taylor Görtler vortices can be obtained by the method of Graftieaux (Graftieaux et al., 2001). One of vortices at Mach disk position is lo cated at (Y, Z) = (0.196, 0.821) mm. In upstream (X = 0.2 mm) of this position, the Görtler number is studied, noted *SC* (*vortex*) in Table 2.

The Eq. (6) can be used to estimate the curvature radius ς by using the jet diameter variation in the flow direction shown in Fig. 8.

$$\varsigma = \left| \frac{(1 + d'^2)^{1.5}}{d''} \right|. \tag{6}$$

d': the differential function of the jet diameter in the flow direction; d'': the second differential function of the jet diameter in the flow direction. The momentum thickness δ is estimated by Eq. (7). υ: the local velocity (m/s); U: the velocity in the centre of the flow.

$$\delta = \int \frac{\upsilon}{U}\left(1-\frac{\upsilon}{U}\right)dy. \tag{7}$$

The Görtler number at different radial positions is computed, see in Table 2. The value of the Görtler number can reach into the hundreds, it means that the Taylor Görtler instability exists in the jets. The Görtler number decreases with the decrease in the nozzle diameter for the round cross section nozzles. The vortices in inclined direction are stronger than the opposite direction for Y45 case. For SC case, the value G of the localisation of vortices is higher than the reference case but the values in other two positions are smaller. The similar phenomenon is shown in SR case, the value in Z direction (in which the vorticity is most intensive) is higher than the reference one where the others are smaller. It is not clearly to conclude the strength of Taylor Görtler instability according to these values of Görtler number, because the Görtler number varies significantly with the different positions. Therefore, the Görtler number is not enough to identify the strength of Taylor Görtler instability. In order to observe the counter rotating pair vortices, the

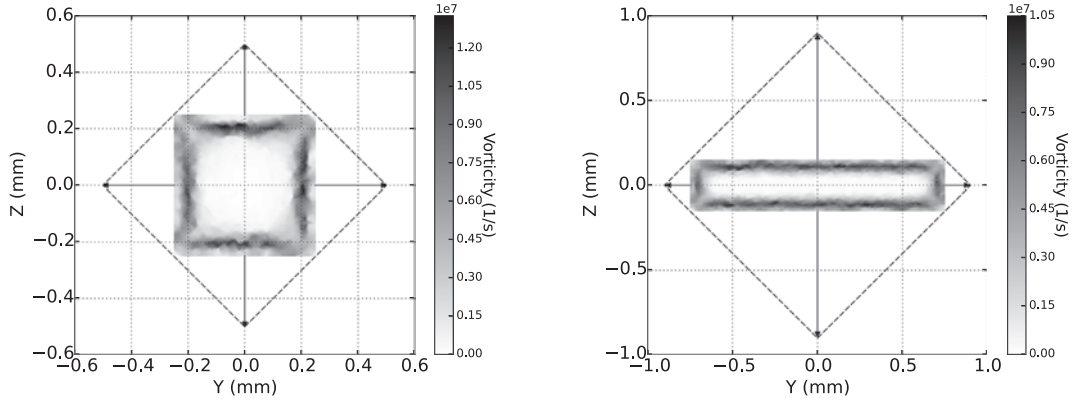

(a) SC (b) SR

Fig. 13. Vorticity distribution over cross-section nozzle of square and rectangular cases.

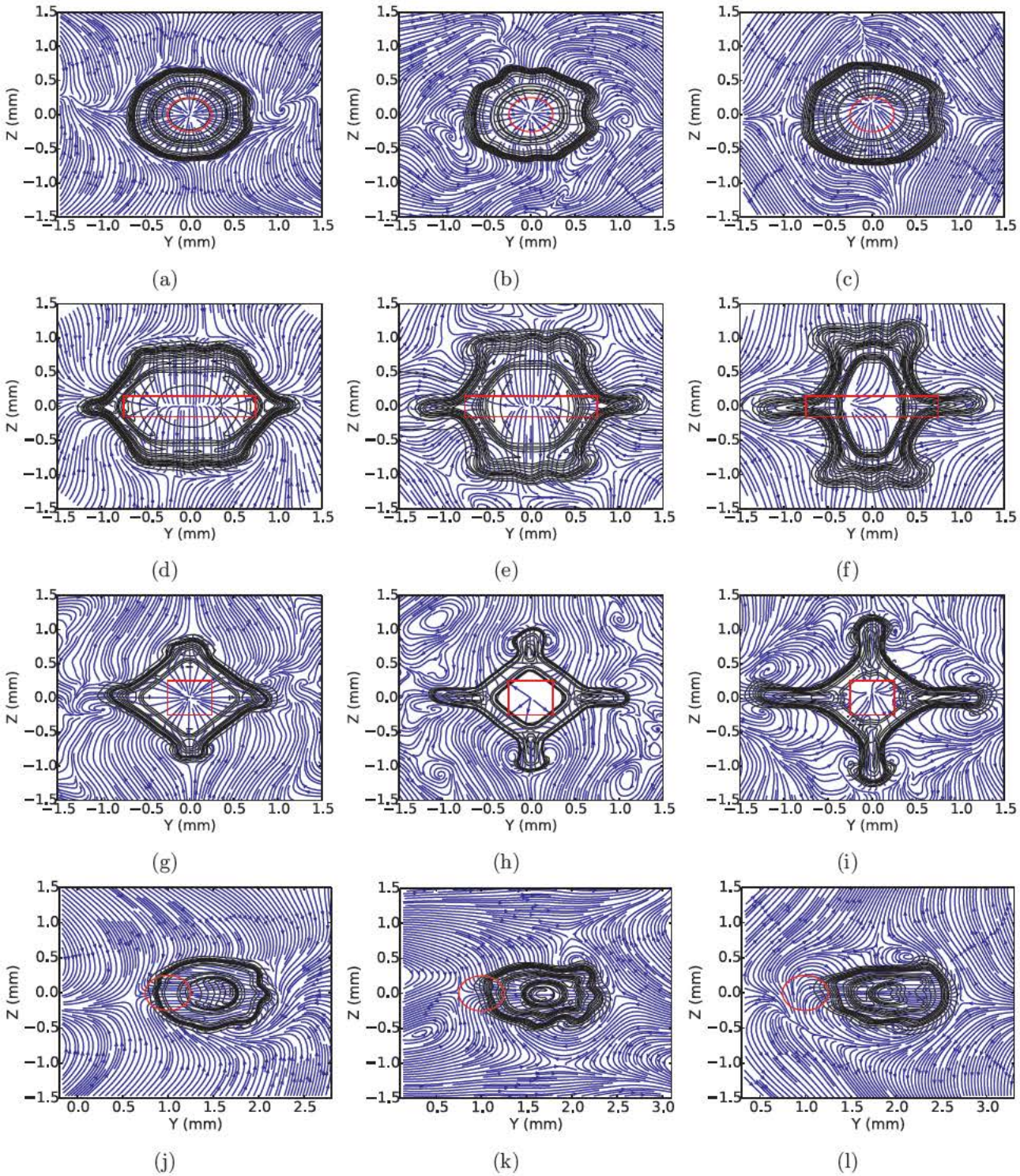

Fig. 14. Streamline and total pressure contours at different flow positions. From top to bottom lines are respectively for D5, SR, SC and Y45; from left to right columns are respectively for the position $X/D_N = 2$, $X/D_N = 3$ and $X/D_N = 4$.

streamline of velocity component YZ and the contour of total pressure over the cross section of jet in the different X positions are shown in Fig. 14.

For the round cases, the vortices in counter rotating pair are not observed, an example of the D5 case is shown in Fig. 14a c. For the other cases (SR, SC and Y45), the vortices in counter rotating pair occur upstream of the Mach disk and diffuse downstream of the Mach disk. For the SR case, one pair of counter rotating vortices occurs in down stream of each nozzle edge. The vortices in length edge comes out earlier (X direction) and intensively than the ones in width edge. This vortices pattern is caused by the vorticity distribution inside nozzle, the vorticity enhances the Görtler vortices. For the SC case, one pair of counter rotating vortices occurs in downstream of each nozzle edge as well. The vortices in Z direction are not exactly the same as the ones in Y direction due to the effect of channel wall in Z direction. Differently than the SR case, the Görtler vortices develops latterly in X direction. For exemple at $X/D_N = 4$, the four pair of counter rotating vortices are clearly observed in SC case where the vortices in Z direction of SR case

already diffuse, see in Fig. 14f and Fig. 14i. It means that the higher aspect ratio of nozzle generates the Görtler vortices closer to the nozzle exit. For the Y45 case, the one counter rotating vortex pair is observed at the inclination direction (Y^+). Because the barrel shock in inclination direction is more curved than the one in opposite direction, seen in Fig. 5d.

For the round cross section nozzle cases, the counter rotating pair of vortices in the shear layers are not observed. The nozzle diameter in the studied range has no impact on the Taylor Görtler instability. The rectangular and the square nozzles enhance the vortices in downstream of nozzle edges. It means that the corner of nozzle enhances the Taylor Görtler instability. The inclination of nozzle enhances as well this in stability in the inclined direction. In addition, the Görtler number is not enough to tell the influence of nozzle geometry on the Taylor Görtler instability because the gas flow development in downstream is not symmetric.

4. Conclusion

This paper discusses the simulation of under expanded nitrogen jets injected into an SGHE channel using an LES method. The model re produces the classical structures of highly under expanded jets. The numerical results are in agreement with the empirical correlations which depend on the NPR and the Mach number at the nozzle exit. This work has mainly focused on the influence of the nozzle geometry on under expanded jet structures. The Fanno flow effect and the pressure drops inside the nozzle lead to different NPR and JPR values at the nozzle exit. The different cross section nozzles (rectangular and square nozzles comparing to the circle nozzle) have the lightest influence on NPR and JPR. This point has never been investigated before. Analysis of the NPR and the Mach number at the nozzle exit highlights two classes of under expanded jets.

Rectangular and square cross section nozzles increase the distance between the nozzle exit and the Mach disk localization. This is due to the divergent feature of the barrel shock of the SR case on the one hand, and the reflected shock waves of the SC case on the other hand. Despite these cases having the same hydraulic diameter compared with the reference case D5, the Mach disk diameter of these cross section shapes is reduced. Furthermore, the nozzle's aspect ratio has a significant in fluence on the distance between the nozzle and the Mach disk. The nozzle inclined at 45° in the Y^+ direction decreases the distance be tween the nozzle exit and the Mach disk localization. This kind of nozzle also decreases the Mach disk diameter D_{DM}. This is caused by the strongest pressure drops inside the nozzle and the inclination angle. The D1 case is excessively influenced by the target wall. The nozzle locali zation has no significant effect on the structures of under expanded gas jets.

The jet diameter in the flow direction is identified by using the radial profile of total pressure. The jet diameter increases the most in the SR and SC cases. The increase in the mass flow rate occurs at the distance of around one nozzle diameter from the nozzle exit. This is due to the entrainment of the ambient gas. From this position, the mass flow rate decreases and once again reaches the initial value. This is another new key point that has never been studied before, but it is important data for the technology of gas mass flow rate detection in SGHE acci dent scenarios.

The momentum pattern over the cross section is identical to the total pressure pattern. The variation in the total pressure radial profile trend is in agreement with that observed in the experiments (Zapryagaev et al., 2010). The cross section structures of the square nozzle are in cross shape. However, the jet through a rectangular nozzle develops more intensively in the width direction than in the length direction. The non homogeneous distribution of vorticity inside the nozzle makes it possible to explain the cross section shape of the jet for the SR and SC cases.

The Görtler number is not enough to distinguish the intensity of Taylor Görtler instability in this study because of the asymmetric gas flow development. The Taylor Görtler vortices are not observed in the round nozzle cases. The four counter rotating vortex pairs of Taylor Görtler instability are clearly observed in downstream of nozzle edges for square and rectangular nozzles. The Taylor Görtler vortices are lo cated in the inclined direction for inclined nozzle.

Acknowledgements

The present work has been carried out by the collaboration between the Atomic Energy and Alternative Energies Commission Cadarache and Toulouse Fluids Mechanisms Institute. The research for this paper was financially supported by the TECNA project.

References

Addy, A.L., 1981. Effects of axisymmetric sonic nozzle geometry on mach disk characteristics. AIAA J. 19, 121–122.
Antsupov, A.V., 1974. General properties of underexpanded and overexpanded supersonic gas jets. Sov. Phys. Tech. Phys 19, 234–238.
Antsupov, A.V., Ivanov, A.V., Karpman, I.M., Traskovskii, V.D., Yudelovich, M.Ya., 1970. Flow in supersonic viscous underexpanded jet. Fluids Dyn. 5, 409–414.
Arnette, S.A., Samimy, M., Elliott, G.S., 1993. On streamwise vortices in high reynolds number supersonic axisymmetric jets. Phys. Fluids 5, 187–202.
Avduevskii, V.S., Ivanov, A.V., Karpman, I.M., Traskovskii, V.D., Yudelovich, M.Ya., 1970. Flow in supersonic viscous underexpanded jet. Fluids Dyn. 5, 409–414.
Cavaro, M., 2010. Apport de l'accoustique non linraire la caractrisation de l'engagement du sodium liquide: application aux racteurs nuclaires de quatrime gnration. [Ph.D. thesis]. Aix Marseille 2 and CEA Cadarache.
Colin, Olivier, Rudgyard, Michael, 1993. High-order Taylor-Galerkin methods for non-linear multidimensional problems. Finite Elem. Fluids.
Colin, Olivier, Rudgyard, Michael, 2000. Development of high-order Taylor-Galerkin schemes for les. J. Comput. Phys. 162, 338–371.
Cook, Andrew W., Cabot, William H., 2005. Hyperviscosity for shock-turbulence interactions. J. Comput. Phys. 203, 379–385.
Crist, S., Sherman, P.M., Glass, D.R., 1966. Study of the highly underexpanded sonic jet. AIAA J. 4, 68–71.
Cumber, P.S., Fairweather, M., Falle, S.A.E.G., Giddings, J.R., 1994. Predictions of the structure of turbulent, moderately underexpanded jets. J. Fluids Eng. 116, 707–713.
Cumber, P.S., Fairweather, M., Falle, S.A.E.G., Giddings, J.R., 1995. Predictions of the structure of turbulent, highly underexpanded jets. J. Fluids Eng. 117, 599–604.
Dam, N.J., Rodenburg, M., Tolboom, R.A.L., Stoffels, G.G.M., Huisman Kleinher-enbrink, P.M., Ter Meulen, J.J., 1998. Imaging of an underexpanded nozzle flow by uv laser rayleigh scattering. Exp. Fluids 24, 93–101.
Dauptain, A., Cuenot, B., Gicquel, L.Y.M., 2010. Large eddy simulation of stable supersonic jet impinging on flat plate. AIAA J. 48, 2325–2338.
Dauptain, A., Gicquel, L.Y.M., Moreau, S., 2012. Large eddy simulation of supersonic impinging jets. AIAA J. 50, 1560–1574.
Donalson, C.D., Snedeker, R.S., 1971. A study of free jet impingement. Part 1. Mean properties of free and impinging jets. J. Fluid Mech. 45, 281–319.
Donalson, C.D., Snedeker, R.S., Margolis, D.P., 1971. A study of free jet impingement. Part 2. Free jet turbulent structure and impingement heat transfer. J. Fluid Mech. 45, 477–512.
Gicquel, L., 2010. Etude des mécanismes et cinétiques d'interactions sodium-CO_2: contribution l'évaluation d'un système de conversion d'énergie au CO_2 supercritique pour les réacteurs rapides caloporteur sodium. [Ph.D. thesis]. Applicable Sciences Nationnal Institut of Rouen and CEA Cadarache.
Görtler, TH., 1954. On the three-dimensional instability of laminar boundary layers on concave walls. Technical memorandum 1, National Advisory Committee for Aeronautics. National Advisory Committee for Aeronautics, Washington. Technical memorandum 1375.
Graftieaux, L., Michard, M., Grosjean, N., 2001. Combining piv, pod and vortex identification algorithms for the study of unsteady turbulent swirling flows. Meas. Sci. Technol 12, 1422–1429.
Hatanaka, K., Saito, T., 2012. Influence of nozzle geometry on underexpanded axisymmetric free jet characteristics. Shock Waves 22, 427–434.
Heeb, N., Gutmark, E., Kailasanath, K., 2014. An experimental investigation of the flow dynamics of streamwise vortices of various strengths interaction with a supersonic jet. Phys. Fluids 26, 086102.
He, M.S., Qin, L.Z., Liu, Y., 2015. Oscillation flow induced by underwater supersonic gas jets from a rectangular laval nozzle. Proc. Eng. 99, 1531–1542.
Holmen, V., 2012. Methods for vortex identification. [M.S. thesis]. Lund University.
Kida, S., Miura, H., 1998. Identification and analysis of vortical structures. Eur. J. Mech. B/Fluids 17, 471–488.
Kolr, V., 2007. Vortex identification: new requirements and limitations. Int. J. Heat Fluid flow 28, 638–652.
Kudoh, H., Sugiyama, K.I., Narabayashi, T., Ohshima, H., Kurihara, A., 2013. Visualization on the behavior of inert gas jets impinging on a single glass tube submerged in liquide sodium. J. Nucl. Sci. Technol. 50, 72–79.
Lécume, S., Carreau, L., Gbahoué, J.L., Roger, F., 1989. Visualisation des modes de propagation de l'énergie dans un jet chauffé non réactif. In: Bertrand, et al. (Eds.),

Rec. Progr. Gén. Proc., Toulouse, 3. pp. 595–600.
Lewis Jr, C.H., Carlson, D.J., 1964. Normal shock location in underexpanded gas and gas-particle jets. AIAA J. 2, 776–777.
Liepman, D., Gharib, M., 1992. The role of streamwise vortices in near-field entrainment of round jets. J. Fluid Mech. 245, 643–667.
Love, E.S., Grigsby, C.E., Lee, L.P., Woodling, J.M., 1959. Experimental and theoretical studies of axisymmetric free jets. Technical Report R-6 NASA.
Moin, P., Kim, J., 1985. The structure of the vorticity field in tur- bulent channel flow part 1: analysis of instantaneous fields and statistical correlations. J. Fluid Mech. 155, 441–464.
Nicoud, F., Ducros, F., 1999. Fluorescence imaging of underexpanded jets and comparison with cfd. Flow Turbul. Combust. 62, 183–200.
Roger, F., Carreau, J.L., Gbahoué, L., Hobbes, P., Allou, A., Beauchamp, F., 2014. Structure of strongly underexpanded gas jets submerged in liquids -application to the wastage of tubes by aggressive jets. Nucl. Eng. Des. 273, 119–130.
Totoda, K., Hiramoto, R., 2006. Effect of streamwise vortices on characteristics of jets. JSME Int. J. 49, 884–889.
Vivaldi, D., 2013. Modeling of underexpanded reactive CO2-into-sodium jets, in the frame of sodium fast reactors. [Ph.D. thesis]. Ecole Nationale Superieure des Mines de Saint-Etienne and CEA Cadarache.
Vuorinen, V., Yu, J., Tirunagari, S., Kaario, O., Larmi, M., Duwig, C., 2013. Large eddy simulation of highly underexpanded transient gas jets. Phys. Fluids 25, 016101.
Zapryagaev, V.I., Kavun, I.N., Kiselev, N.P., 2010. Flow structure at the initial section of a supersonic jet exhausting from a nozzle with chevrons. J. Appl. Mech. Tech. Phys 51, 202–210.
Zapryagaev, V.I., Kavun, I.N., Kiselev, N.P., 2010. Structure of supersonic jets with vortex generators at the nozzle exit. Int. J. Aerospace Innov. 2, 202–210.
Zhou, J., Adrian, R.J., Balachandar, S., Kendall, T.M., 1999. Mechanisms for generation coherent packets of hairpin vortices in channel flow. J. Fluid Mech. 387, 353–396.